ISNN:2181-1296

SHAROF RASHIDOV NOMIDAGI
SAMARQAND DAVLAT UNIVERSITETI

САМАРКАНДСКИЙ ГОСУДАРСТВЕННЫЙ
УНИВЕРСИТЕТ ИМЕНИ ШАРОФА РАШИДОВА

SAMARKAND STATE UNIVERSITY NAMED
AFTER SHAROF RASHIDOV

ILMIY AXBOROTNOMA

НАУЧНЫЙ ВЕСТНИК
SCIENTIFIC JOURNAL

ANIQ VA TABIIY FANLAR SERIYASI

Matematika, Mexanika, Informatika
Fizika, Kimyo, Biologiya, Geografiya

№ 3/2 (151)
2025

ISSN 2181-1296

ILMIY AXBOROTNOMA

НАУЧНЫЙ ВЕСТНИК SCIENTIFIC JOURNAL

2025-yil, 3-son (151/2) ANIQ VA TABIIY FANLAR SERIYASI

Matematika, Mexanika, Informatika, Fizika, Kimyo, Biologiya, Geografiya

Samarqand viloyat matbuot boshqarmasida ro‘yxatdan o‘tish tartibi 09-25.
Jurnal 1999-yildan chop qilina boshlagan va OAK ro‘yxatiga kiritilgan.

BOSH MUHARRIR **R. I. XALMURADOV, t.f.d., professor**
BOSH MUHARRIR O‘RINBOSARLARI: **H.A. XUSHVAQTOV, f-m.f.d., dotsent**

TAHRIRIYAT KENGASHI:

Sh.A.Alimov	- O‘zFA akademigi	**M.X.Ashurov**	- O‘zFA akademigi
S.N.Lakayev	- O‘zFA akademigi (SamDU)	**B.J.Axmedov**	- O‘zFA akademigi
M.M.Kamilov	- O‘zFA akademigi	**Q.G‘.G‘ulomov**	- O‘zFA akademigi
A.G.Yagola	- Moskva davlat universiteti professori (Rossiya)	**A.A.Zaxidov**	-Texas Nanotexnologiya instituti professori (AQSh)
Alberto Del Bimbo	-Florensiya universiteti professori (Italiya)	**N.B. Ferapontov**	- Moskva davlat universiteti professori (Rossiya)
Sh.Tugizov	-Kaliforniya universiteti professori (AQSh)	**V.L.Popov**	-Berlin texnika universiteti professori (Germaniya)
A.S.Soleev	- f.-m.f.d., professor (SamDU)	**N.F.Bunkin**	- Moskva davlat texnika universiteti professori (Rossiya)
I.A.Ikromov	- f.-m.f.d., professor (SamDU)	**Haji Akber Aisa**	-Xinjiang tibbiyot universiteti professori (Xitoy)
B.X.Xo‘Jayarov	- f.-m.f.d., professor (SamDU)	**E. A. Abduraxmonov**	- k.f.d., professor (SamDU)
L.Sabirov	-f.-m.f.d., professor (SamDU)	**N. K. Muxamadiyev**	- k.f.d., professor (SamDU)
A.Jumaboyev	-f.-m.f.d., professor (SamDU)	**L. A. Bulavin**	- Kiev milliy universiteti
X.Bozorov	-k.f.d., professor (SamDU)	**X. Q. Xaydarov**	- b.f.d., professor (SamDU)
O.Q.Quvondiqov	-f.-m.f.d. professor (SamDU)	**Z. I. Izzatullayev**	- b.f.d., professor (SamDU)
A.Z.Xasanov	-f.-m.f.d. professor (SamDU)	**A.B.Hasanov**	-tex.f.d., professor (SamDU)
Muhammad Suzuri bin Hitam	- Terengganu universiteti professori (Malayziya)	**Sh. T. Xoliqulov**	- q.-x.f.d., professor (SamDU)
K.D.Kuliyev	- f.-m.f .n. professor (SamDU)	**S. B. Abbosov**	- g.f.d., professor (SamDU)
A.M.Xolxo‘jayev	-f.-m.f.d., professor (SamDU)	**M.E. Mo‘minov**	-f.-m.f.d., professor (SamDU)
J.Abdullayev	-f.-m.f.d., professor (SamDU)	**I.I.Jumanov**	-tex.f.d., professor (SamDU)
A.R.Axatov	-tex.f.d., professor (SamDU)	**N.S.Mamatov**	-tex.f.d., professor (TIQXMMI)
D.B.Xursanov	- g.f.f.d., dotsent (SamDU)	**A.Sh.Yarmuxamedov**	-f-m.f.n., dotsent (SamDU)
F.Nazarov	-tex.f.f.d., dotsent (SamDU)	**X.S.Xaydarov**	-f-m.f.n., dotsent (SamDU)

Obuna indeksi – yakka tartibdagi obunachilar uchun **- 5583,**
tashkilot, korxonalar uchun **- 5584**

M U N D A R I J A
C O N T E N T S

№	Maqola nomi	Article title	Bet/ page
1	Kasr psevdoparabolik tenglama uchun Samarskiy-Ionkin ikki nuqtali chegaraviy shartlar **Sagdullaeva M.U., Xasanov G.A., Yuldashev T.K.**	Samarskii-Ionkin two-point boundary conditions for a fractional pseudoparabolic equation **Sagdullaeva M.U., Khasanov G.A., Yuldashev T.K.**	**5-14**
2	Gerasimov-Kaputo turidagi kasr tartibli nochiziqli differensial tenglamalar **Shukurova M.D., Xasanov G.A., Yuldashev T.K.**	Nonlinear differential equation with Gerasimov-Caputo type fractional operator and degenerator **Shukurova M.D., Khasanov G.A., Yuldashev T.K.**	**15-22**
3	NaH da lazer ta'sirida dissotsiatsiya dinamikasi **Umarov O., Jumabaev A.**	Laser-induced dissociation dynamics in NaH **Umarov O., Jumabaev A.**	**23-30**
4	Radon transformasidan foydalanish, tasvirni tanishda aylana sfera proyeksiyasini yaratish **Khatamov O., Mamanova B.**	Using the radon transform to create a projection of a circular sphere in image recognition **Khatamov O., Mamanova B.**	**31-38**
5	Flavonoid komplekslarining metal ionlari bilan sintezi, spektroskopik tadqiqotlar va supramolekulyar tizimlar **Ergashova Sh., Muxamadiyev N.**	Synthesis of flavonoid complexes with metal ions, spectroscopic studies and supramolecular systems **Ergashova Sh., Mukhamadiev N.**	**39-45**
6	2-benzil-6,7-dimetoksi-1,2,3,4-tetragidroizoxinolin hosilalari sintez reaksiyalarini o'rganish **Suyunova S.N., Quljonov J.X., Xudoyberdiyeva A.A., Urunbayeva Z.E. Z.E., Saidov A.Sh., Vinogradova V.I.**	Study of the reactions of synthesis of 2-benzyl-6,7-dimethoxy-1,2,3,4-tetrahydroisochinoline derivatives **Suyunova S.N., Kuljonov J.X., Khudoyberdieva A.A., Urunbaeva Z.E. Z.E., Saidov A.Sh., Vinogradova V.I.**	**46-50**
7	Keyingi qo'shni tugunlargacha o'zaro ta'sirlanuvchi ikki bozonli panjara gamiltoniani **Axmadova M., Axmatova Sh.**	A two-boson lattice hamiltonian with interactions up to next-neighboring sites **Akhmadova M., Akhmatova Sh.**	**51-58**
8	Sekin aylanishli magnitlangan neytron yulduzlarning plazma magnitosferasi o'zgartirilgan gravitatsiyada **Sayfiyev Sh.**	Plasma magnetosphere of slowly rotating magnetized neutron stars in modified gravity **Sayfiev Sh.**	**59-65**
9	Vaqtli qatorlar va mashinaviy o'qitish asosida sotuvdagi kechikishlarni aniqlash usullari **Nazarov F., Sayidqulov A.**	Methods for detecting delays in sales based on time series and machine learning **Nazarov F., Sayidkulov A.**	**66-71**
10	Integrallashgan matematik modellar va ularning qo'llanilishi **Safarov R., Xudoyberdiyev S.I.**	Integrated mathematical models and their applications **Safarov R., Khudoyberdiyev S.I.**	**72-77**
11	Chekli zichlikka va qator ko'rinishdagi moslangan manbaga ega Hirota tenglamasi uchun boshlang'ich qiymat masalasi **Eshbekov R.**	The initial value problem for the Hirota equation with finite density and self-consistent series source **Eshbekov R.**	**78-84**
12	L-sistein bilan modifikatsiyalangan mezog'ovak silikagel yordamida og'ir metall kationlarini ajratish **Ulugboyeva G.O., Kuliboyeva N.Sh., Uzokov J.R., Fazliyeva N.T., Muxamadiev N.Q.**	Removal of heavy metal cations using mesoporous silicagel modified with L-cysteine **Ulugboeva G.O., Kuliboeva N.Sh., Uzokov J.R., Fazlieva N.T., Mukhamadiev N.Q.**	**85-90**
13	Titan nano oksidi sintezi va uning fotokatalitik xossalarini zarracha o'lchamiga bog'liqligi **Mamaziyeva S., Avazova N., Tashmatova R., Muxamadiev N., Muxamadiev A., Uzokov J.**	Synthesis of nano titanium oxide and dependence of its photocatalytic properties on particle size **Mamazieva S., Avazova N., Tashmatova R., Mukhamadiev N., Mukhamadiev A., Uzokov J.**	**91-96**
14	$SrTiO_3$ nanozarrachalarini sintez qilish va ularning o'lcham-fotokatalitik xossalari **Hayitova M., Baxranova M.A., Muxamadiyev N.Q.**	Synthesis of $SrTiO_3$ and its size-dependent photocatalytic properties **Hayitova M., Bakhranova M.A., Mukhamadiyev N.Q.**	**97-102**

№	Maqola nomi	Article title	Bet/ page
15	Rekreatsiya maqsadlarida tabiatdan foydalanishni boshqarish **Rafikova N.**	Management of nature utilization for recreational purposes **Rafikova N.**	**103-110**
16	Modifikatsiyalangan faollashgan ko‘mir yordamida eritma tarkibidagi organik bo‘yoqlarni ajratish **Ergasheva D., Muxamadiyev A., Muxamadiyev N., Uzokov J.**	Separation of organic dyes from solutions using modified activated carbon **Ergasheva D., Mukhamadiyev A., Mukhamadiyev N., Uzokov J.**	**111-116**
17	Neyron tarmoqli modellar asosida qandli diabetni tashxislashning intellektual algoritmlari **Sariyev Sh.N.**	Intelligent algorithms for diagnosing diabetes mellitus based on neural network models **Sariev Sh.N.**	**117-123**
18	Mahalliy kaolindan seolitlar sintez va fizik-kimyoviy tahlili **Magdiev Sh., Majidova F., Nasimov A., Tashpulatov X., Toshpulatov D., Mirzayev Sh., Norboev K., Normuradov O.**	Synthesis and physicochemical analysis of zeolite from local kaolin **Magdiev Sh., Majidova F., Nasimov A., Tashpulatov Kh., Toshpulatov D., Mirzaev Sh., Norboev K., Normuradov O.**	**124-129**
19	Densenet modelini transfer o‘qitish asosida masofadan zondlash sahnalarini tasniflash aniqligini oshirish maqolaning o‘zbek tilidagi nomi **Yusupov O.R., Eshonqulov E.Sh.**	Enhancing the accuracy of remote sensing scene classification using transfer learning with densenet **Yusupov O.R., Eshonkulov E.Sh.**	**130-144**
20	Neft va gaz quduqlari minerallashgan qatlam suvlarining kimyoviy tarkibi va fizik-kimyoviy xususiyatlarini o‘rganish **Kenjaev N.A., Igamkulova N.A.**	Chemical composition and physico-chemical properties of mineralized formation waters from oil and gas wells **Kenjaev N.A., Igamkulova N.A.**	**145-148**

UDC: 535.012 **DOI:https://doi.org/10.59251/2181-3973.2025.v1.138.1.3565**

LASER-INDUCED DISSOCIATION DYNAMICS IN NaH

O.Umarov[1,2], A.Jumabaev[2]
[1]University of Debrecen, Bem tér 18, 4026, Debrecen, Hungary.
[2]Samarkand State University named after Sharof Rashidov, Samarkand, Uzbekistan.

O.Umarov University of Debrecen, Bem tér 18, 4026, Debrecen, Hungary.

Received: 07.06.2025
Revised: 26.06.2025
Accepted: 10.07.2025
Published: 31.07.2025

Publisher: Samarkand State University named after Sharof Rashidov.

Abstract. It is known that electronic conical intersection (or degeneracy between potential energy surfaces) can be created by laser or quantum lights, even in diatomic molecular systems. In order to examine the impact of the light-induced conical intersection (LICI), we perform numerical simulations to explore molecular photo-dissociation dynamics in the presence of several LICIs created by an electromagnetic laser field. Dissociation dynamics of the sodium hydride (NaH) molecule with the lowest three electronic states are explained by analyzing values of the dissociation yields and angular distributions of molecular photo-fragments. The one-dimensional time-dependent Schrödinger equation (TDSE) is applied to study molecular dynamics in the Multi-configuration time-dependent Hartree (MCTDH) method.

Keywords: conical intersection, laser field, non-adiabatic coupling, photo-dissociation dynamics.

NaH da lazer ta’sirida dissotsiatsiya dinamikasi

Annotatsiya. Ma’lumki, elektron konussumon kesishish (yoki potensial energiya sirtlari orasidagi buzilish) hatto ikki atomli molekulyar tizimlarda ham lazer yoki kvant nurlari tomonidan yaratilishi mumkin. Yorug‘lik ta’sirida yaratilgan konussumon kesishishning (LICI) ta’sirini o‘rganish uchun elektromagnit lazer maydoni tomonidan yaratilgan bir nechta LICI lar mavjudligida biz molekulyar photo-dissosiasiya dinamikasini o‘rganish uchun raqamli hisob-kitoblarni bajaramiz. Dissosilanish qiymati va molekulyar photo fragmentlarning burchak taqsimoti qiymatlarini tahlil qilish orqali eng past uchta elektron sathga ega bo‘lgan natriy gidrid (NaH) molekulasining dissosilanish dinamikasi tushuntiriladi. Molekulaning dinamikasini o‘rganish uchun bir o‘lchovli vaqtga bog‘liq Shredinger tenglamasi (TDSE) ko‘p konfigurasiyali vaqtga bog‘liq Hartree (MCTDH) usulida echiladi.

Kalit so‘zlar. konussimon kesishish, lazer maydoni, adiabatik bo‘lmagan bog‘lanish, photodissosiasiya dinamikasi.

Динамика лазерно-индуцированной диссоциации в NaH

Аннотация. Известно, что электронное коническое пересечение (или вырождение между поверхностями потенциальной энергии) может быть создано лазерным или квантовым светом даже в диатомарных молекулярных системах. Чтобы изучить влияние светоиндуцированного конического пересечения (LICI), мы проводим численное моделирование динамики фотодиссоциации молекул в присутствии нескольких LICI, созданных электромагнитным лазерным полем. Динамика диссоциации молекулы гидрида

натрия (NaH) с тремя низшими электронными состояниями объясняется на основе анализа значений выходов диссоциации и угловых распределений молекулярных фотофрагментов. Одномерное уравнение Шредингера, зависящее от времени (TDSE), применяется для исследования молекулярной динамики в многоконфигурационном методе Хартри, зависящем от времени (MCTDH).

Ключевые слова. коническое пересечение, лазерное поле, неадиабатическая связь, динамика фотодиссоциации.

I. Introduction. To study molecular dynamical properties, one relies on one of the fundamental methods, the Born-Oppenheimer approximation (BOA) [1], which allows us to separately study the fast-moving electrons and slow-moving nuclei. However, the BOA becomes invalid when a molecular system has non-adiabatic processes [2-3]. In non-adiabatic phenomena, molecular potential energy surfaces may intersect or approach enough to each other. The former type of intersection is called conical intersection (CI), while the latter case is called avoided crossing (AC) [4]. In such a case, an efficient funnel appears to transfer energy from one surface to another, and these processes directly or indirectly affect molecular spectroscopy, dissociation dynamics and topological features of molecules.

Unlike natural non-adiabatic phenomena, light-induced ones emerge when an external field, such as a classical laser pulse or quantum cavity, is exposed to a molecular system to couple electronic (even rovibrational eigenstates) states [5]. In this case, intersection so-called light-induced conical intersection might be formed as the external field couples electronic states, even in diatomics where natural CI does not appear because of possessing only one degree of freedom (DOF). On the other hand, the coupling strengths between electronic states and the positions of LICIs in molecular systems can be controlled by changing the frequencies and intensities of the laser field. Both natural and light-induced processes can allow us to create molecular types of equipment like photoswitchable molecules or photoprotecting devices collecting high-density data storage at degeneracy points in molecules.

As is well established, the sodium hydride molecule plays a pivotal role in astrophysics, with its photo-dissociation being a predominant mechanism for its destruction in interstellar clouds. Multiple experimental and theoretical studies of the NaH system are dedicated to both classical and quantum lights [6-8]. The present work is a continuation of our previous work [8]. In the former paper, photo-dissociation dynamics are investigated along with photo-fragment kinetic energy release (KER) spectra and angular distributions in both 1D and 2D models for the fixed parameters of the pump and probe pulses. However, this work investigates dissociation processes with different laser parameters in a 1D framework. Conducting calculations of fragment angular dissociations helps us better understand the dissociation dynamics of the system.

II. Methodology and theoretical background. The NaH molecule is hetronuclear system therefore has significant permanent dipole moments (PDMs) of each electronic states. The impact of the system's PDM was studied in our previous work **[**see for the detailed explanation [8]. In that paper, molecular electronic structure calculations (potential energies surfaces (PESs), PDMs and transition dipole moments (TDMs)) were performed for the lowest three electronic states using the multireference configuration interaction (MRCI) method at the aug-cc-pV5Z level in the Molpro quantum package [9]. Because the MRCI method can simultaneously consider dynamical and static electron correlations, it has been chosen to solve the time-independent problem, which suits this system related to non-adiabatic phenomena. Figure 1 displays the PESs and schematic view of the pump and probe pulses. The solid red, blue and green curves in Fig. 1 correspond to the relevant potential energy surfaces V_X ($X^1\Sigma^+$), V_A ($A^1\Sigma^+$), and V_B ($B^1\Pi$), respectively, labeled as X, A and B throughout the paper (the full description of Figure 1 will be given later in this section).

After the time-independent problem for this system is solved, we can move on to solve the time-dependent problem, which is the TDSE. The full Hamiltonian (H_{full}) comprises two parts: molecular Hamiltionian (H_m) and light-matter interaction part of the Hamiltonian, $H_{lm} = E_{full}(t) \cdot d(R)$. Since three electronic states are considered in the calculations, the 3X3 matrix representation of the full Hamiltonian takes the following form:

$$H_{full} = \begin{pmatrix} \frac{-1}{2}\frac{\partial^2}{\partial R^2} + V_X & 0 & 0 \\ 0 & \frac{-1}{2}\frac{\partial^2}{\partial R^2} + V_A & 0 \\ 0 & 0 & \frac{-1}{2}\frac{\partial^2}{\partial R^2} + V_B \end{pmatrix} + E_{full}(t) \begin{pmatrix} d_X cos(\theta) & d_{XA} cos(\theta) & d_{XB} sin(\theta) \\ d_{AX} cos(\theta) & d_A cos(\theta) & d_{AB} sin(\theta) \\ d_{BX} sin(\theta) & d_{BA} sin(\theta) & d_B cos(\theta) \end{pmatrix} \quad (1)$$

where $\frac{-1}{2}\frac{\partial^2}{\partial R^2}$ is the molecular vibrational kinetic energy operator. R and (θ) represent the molecular vibrational and rotational coordinates, respectively, where θ is the angle between the molecular axis and polarization direction of the EM field. The direction of the TDM between X and A is parallel (cos(θ) in off-diagonal elements of Eq. 1), while the directions of the TDMs between X and B as well as A and B are perpendicular to each other (sin(θ) in off-diagonal elements of Eq. 1). μ_r is the reduced mass of the electrons.

The full EM field $E_{full}(t)$ (in Eq. (1)) comprises two parts, pump and probe laser pulses:

$$E_{full}(t) = E_{pm} g_{pm}(t) cos(\omega_{pm} t) + E_{pr} g_{pr}(t) cos(\omega_{pr} t) \quad (2)$$

Here, the first part of Eq. (1) expresses the pump laser field carrying energy ω_{pm} and amplitude E_{pm} (where $E_{pm} = \sqrt{I_{pm}/E_{au}}$, $E_{au} = 3.50944758^{16}$) to transfer the molecular dynamics of the system from the V_X state to the V_A state, while the second part stands for the probe laser field carrying energy ω_{pr} and amplitude E_{pr} can transfer the subsequent population from V_A to the others, V_X and V_B states. $g_{pm}(t)$ and $g_{pr}(t)$ are the envelope functions that give cos-square pulse shapes for the pump and probe pulses, respectively. In the first step, the pump is exploited to transfer some amount of population from the V_X to V_A states. In the second step, the probe is applied with different time delays to transfer the further population from the V_A state to the other two states, V_X and V_B states. As the probe is applied to the system, two LICIs are formed between the ground state and the first excited states and two LICIs between two excited states (see the details in Fig. 1). During the calculations, the energies and pulse durations of the pump and probe are constant, whereas the intensities of both pulses vary for four cases (see **Table 1** for details). For all cases, the position of the pump pulse is fixed, starting from 0 femtoseconds (fs) and ending with 8 fs, whereas the probe pulse is not fixed but varies from 0 up to 316 fs to get various delay times from 0 to 300 fs. The delay time is the time difference between the centers of two pulses.

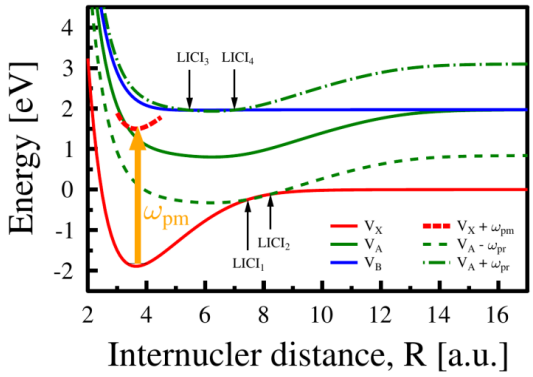

Figure 1. The PESs and schematic view of the pump and probe pulses. The three solid curves are the field-free PESs of each electronic state, while the dashed lines stand for the shifted PESs due to the probe pulse. Four vertical arrows display the positions of the LICIs due to the probe pulse. A cut of a dashed red line shows the position of the transferred wave packets after the pump transfers from the X to the A states.

As for the wave function for the full Hamiltonian, the MCTDH method is described in detail in Reference [10]. During the calculations, the Fast Fourier transformation discrete variable representation (FFT-DVR) is used to describe the vibrational DOF, where the number of grid points is set to N_R =1024 with a range of R=2.0 to 50.0 atomic units (a.u.). For the rotational DOF, Legendre polynomials are

applied in our simulations with N_θ=91. It should be noted that the angular coordinate (θ) is considered a parameter in the 1D framework, whereas it is a variable in the 2D framework. The number of single-particle functions has been selected as $n_R = n_\theta = 10$ for both vibrational and rotational DOFs. All calculations correctly converged with these parameters.

The solution of the TDSE can be employed to calculate the KER spectra and the dissociation probabilities of the individual electronic states using the following equations [11]:

$$P_{ker}(E) = \int_0^\infty dt \int_0^\infty dt' \langle \psi(t)|W|\psi(t')\rangle e^{-E(t-t')} \quad (3)$$

and,

$$P_{diss}(E) = \int_0^\infty dE \cdot P_{ker}(E) \quad (4)$$

where ψ(t) is a nuclear wave function described in the MCTDH method [10]. -iW is complex absorbing potential (CAP) to capture the outgoing wave packets at the last 10 a.u. (from 40 and 50 a.u.) of grid points.

III. Results and discussion.

In this section, the results obtained are discussed in detail. In the first subsection, the dissociation processes are described along with the nuclear wave packet motion on the A state, while the second subsection is devoted to the angular distributions of photo-fragments of the molecule.

III.1. Photo-dissociation processes. Before discussing dissociation dynamics, we have to examine the field-free nuclear wave packet motion on the A state given in Figure 2. The density motion is visualized after the pump (corresponding to the parameters of the 1th calculation in Table 2) is applied to the system (without the probe). The transferred population from X to A starts propagating back and forth on the bound A state with the R≈3 to 10 a.u. range. The horizontal dashed and dotted lines are the location of the LICIs owing to the probe laser, and it is predictable that if the probe is switched on, the wave packets can be transferred through these LICIs from the A to the other two states, X and B ones, according to the non-adiabatic phenomena. The oscillation behaviors of the dissociation yields of the X and B states in Figure 3 are due to the existence of these LICIs.

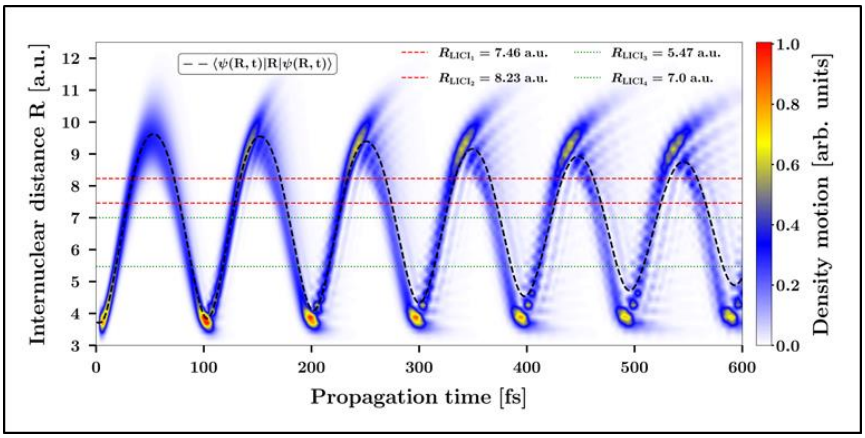

Figure 2. Field-free nuclear wave packet motion on the A state as a function of propagation time. The darker the color, the greater the nuclear density value (on the right-hand side timescale). The horizontal dashed and dotted lines express the locations of the degeneracy points between electronic states. Furthermore, the dashed black line displays the time-dependent expectation value of the internuclear distance.

The dissociation yields can be calculated using Eq. (3) for each electronic state. Figure 3 demonstrates the dissociation probabilities of the lowest three electronic states as a function of delay time (τ) for various pump and probe laser intensities. For the intense pulses (panel (a)) where $I_{pm}=1*10^{13}$W/cm^2 and $I_{pr}=1*10^{12}$W/cm^2, the pump transfers almost 44% and 6.7% of the X state populations to the A and B states, respectively (see Table 2). In the case of the only pump, all transferred populations to the B state experience dissociation, while dissociation does not almost occur in the A and X states. However, when the probe is applied with different positions (to get different delay times), a large amount of populations are transferred to the X state, especially to the B state; eventually, the transferred populations to the X and B states dissociate. The point of $LICI_4$ is more significant than

that of $LICl_3$ because the value of TDM between A and B corresponding to the point of $LICl_4$ is almost twice larger than that of $LICl_3$ (see the TDM's figure in Reference [8]). Therefore, the peaks of the dissociation probabilities on the B state (blue lines in panel (a)) correspond to the time when the wave packet moves around the point of $LICl_4$ as the probe is on. Another noticeable difference in the B state dissociation yields is that the dissociation line starts decreasing after τ=280 fs because of the significant effect of the molecule's rotational motion. The analysis has shown that our molecule starts its rotational motion from about τ=220 fs, and it considerably influences dissociation dynamics as delay time increases. Also, the dissociation occurs on the strong bound ground (X) state owing to the transferred populations made by the probe pulse. The reason for the smaller dissociation on the X state than on the B state is that the transferred populations from A to X not only go to the dissociative range (to the right in Fig. 1) but also go to the bound range (to the left) of the X state to be trapped, not letting go to the dissociative range. The amount of the dissociated population is very small (~ 10^{-5}) because of the bound state.

Figure 3. The dissociation yields of the three electronic states are displayed as a function of the delay time of the τ=0 and τ=300 fs range. The calculations have been done according to the parameters of the pump and probe pulses in Table 1.

As to panels (b)-(d), although their values are very different from each other due to the various

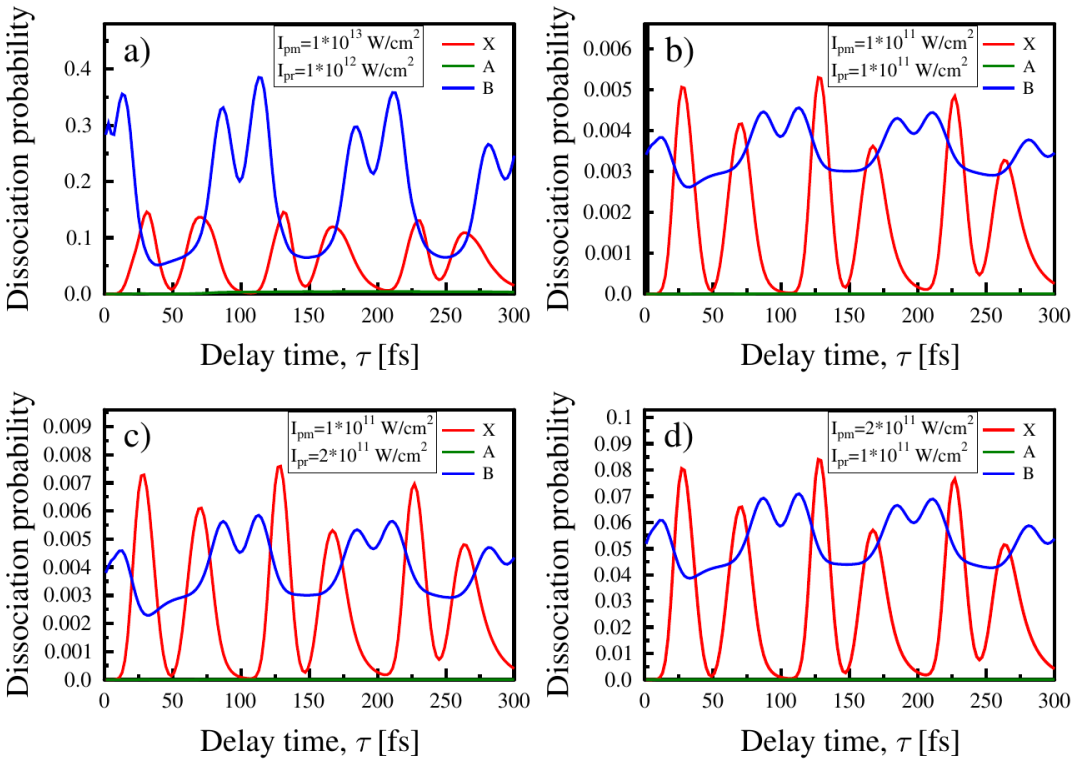

values of pump and probe intensities (Table 1), the shapes of the dissociation probabilities of the X and B states are very similar. Analyses of nuclear densities of each electronic state have shown that in the low probe intensities, most of the transferred population from A to X goes to the dissociative range rather than to the bound range of the X state. The larger population goes to the dissociative range, the more dissociation occurs. As a result, the peak values of the dissociated populations on the X state increased for the low probe intensities, even larger than the peaks of dissociation on the B state (panels (b) to (d)). For the 2nd and 3rd calculations, the probe transfers only 1.1% of the population from X to A and 0.3% from X to B, remaining almost 98.5% of the population on the X state (see Table 2). As a consequence, the dissociation yields on the X and B states decrease considerably compared to panel (a). Of course, the dissociatio yields of X and B increase a little bit (almost 1.5 times) in panel (c) compared to in panel (b) because the probe intensity is two times higher, 2*10^{11} W\cm^2. However, it can be seen that the dissociation yields of X and B in panel (d) are enough higher compared with panels (b) and (c) because the pump transfers about 18.6% of the population from X to A and 4.3% from X to B. The more transferred populations from X to A, the more populations are transferred from

A to B; eventually, they dissociate in the dissociative B state. Similarly, the more transferred populations from X to A, the more molecules are transferred back from A to X through the $LICI_1$ and $LICI_2$ due to the probe effect.

III.2. Photo-fragment angular distributions. To better understand the system's dissociation dynamics, fragment angular distributions of the individual electronic states are discussed as a function of the delay time. The calculations have been conducted between 0 and 90 degrees in the case of the 1D model, where the angle between the pulses' polarization direction and molecular axis is a parameter. Figure 4 shows the angular distributions of the photo-fragment for the ground state as a function of delay time. Panels (a) to (d) correspond to the order of calculations in Table 1. In general, it is clear that there are no populations transferred at around 90 degrees for all panels because of the parallel direction of the TDM between X and A with the polarization direction of the pump ($\cos^2(90^\circ)=0$ in Eq. 1). It might be true only for the case; that is, the 1D model, and the calculations in 2D can be our next project to investigate the effect of the molecular rotational motion on dissociation with different intensities. The locations of the dark round shape in dissociation correspond to the times when the nuclear wave packet motion on the A state moves around the points of $LICI_1$ and $LICI_2$ because, at these times, the probe transfers populations from A to X, and the values of alignment ($\cos^2(\theta)$) increase on these times due to the effect of the probe.

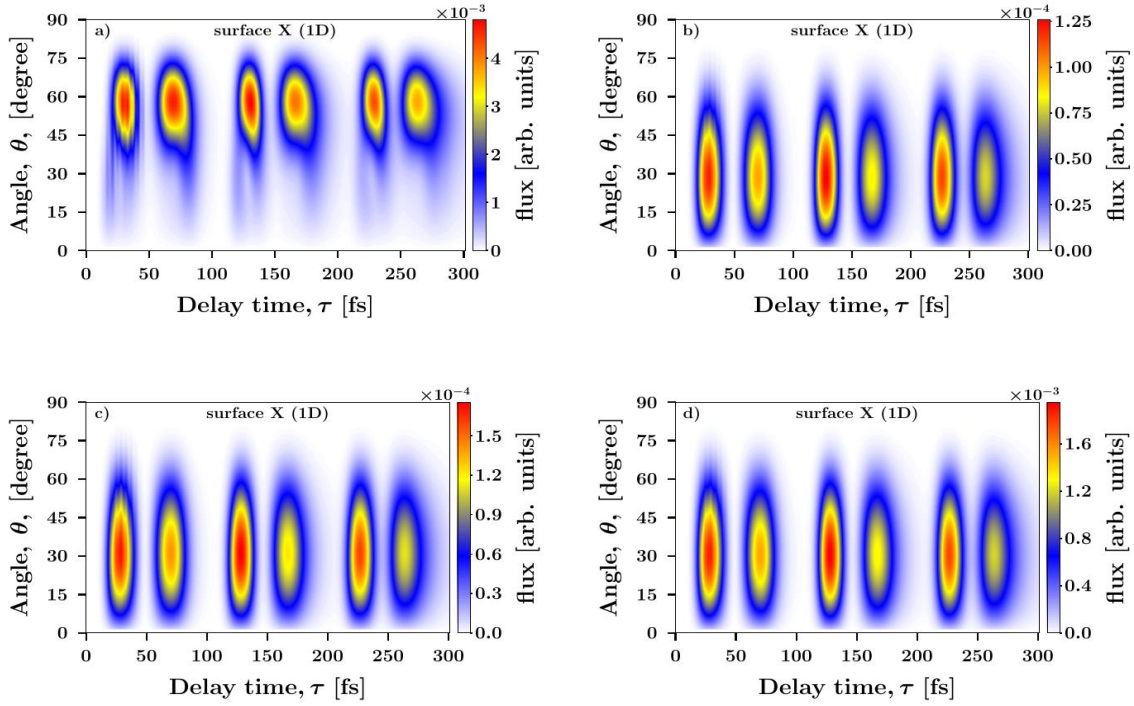

Figure 4. Fragment angular distributions of the NaH system for the ground electronic state are demonstrated as a function of the delay time. The order of the panels (a) to (d) suits the order of the calculations 1-4 in Table 1.

For panel (a), the analysis of the alignment has shown that as the pump and probe are on, they rotate the molecule to the lower direction of θ (from higher direction), increasing the value of the $\cos^2(\theta)$. The alignment varies between about 0.15 and 0.55, and therefore, the dissociation is gathered at around 70 to 45 degrees, in turn. For panels (b) to (d), the spectra are almost identical even though their flux values are very different (on the right side timescale) because the shape of the dissociation probabilities (red lines) of the relevant panels (b) to (d) in Fig. 3 are very similar despite their different values. Another noticeable difference between panel (a) and panels (b)-(d) is the location of the collected dissociation ranges; that is, the dissociation happens between nearly 10 and 60 degrees for panels (b)-(d) in Fig. 4, whereas the dissociative range is around 45 to 70 degrees for panel (a).

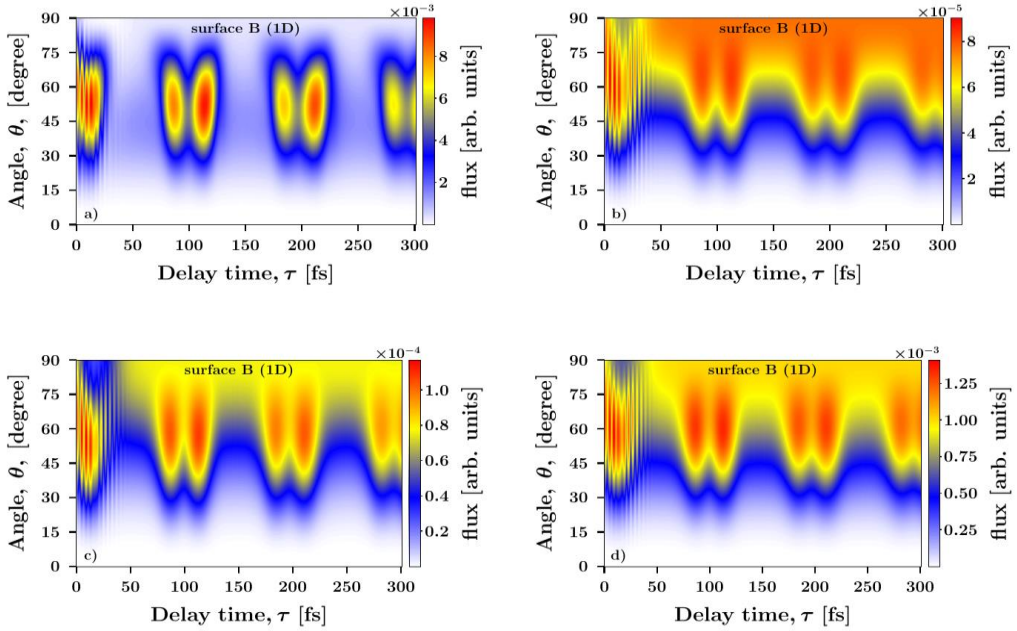

Figure 5. Fragment angular distributions of the NaH system for the second excited electronic state are presented as a function of the delay time. The order of the panels (a) to (d) suits the order of the calculations 1-4 in Table 1.

Fig. 5 demonstrates the angular distributions of the dissociative sodium hydride molecule for the B state. Panels (a) to (d) in Fig. 5 correspond to the order of calculations in Table 1. It can be easily seen that nothing appears around the 0 degrees for all panels because the fact that no populations are transferred from X to B or A to B owing to the perpendicular direction of the TDM between X and B (as well as A and B) with the pump and robe pulses ($\sin^2(90^\circ)=0$ in Eq. 1). In general, no populations are transferred from X to A at 90 degrees due to the parallel direction of the TDM between X and A with polarization direction of the pump. As a consequence, the further populations are not expected from A to B at 90 degrees in 1D. However, for panel (a), a small amount of dissociation happens around 90 degrees because, in this case, the pump transfers around 6.7% of populations of X to directly B, and all dissociate (see Table 2). Although direct population from X to B is very small (0.03% and 4.3%) for the 2nd, 3rd and 4th calculations (panels (b), (c) and (d) in Fig. 5), most of the dissociation happens around 90 degrees for these cases (see panels (b)-(d)). This can be explained by the following: First, the pump builds up the anisotropic angular distribution of populations in the A state and rotates the system. Then, the probe is on, transferring molecules from A to B. The transferred molecules continue to rotate further (on the B state) to the direction of 0 degrees (on the lower adiabatic state) and 90 degrees (on the upper adiabatic state) during the dissociation. For the shorter delay times (up to τ=300 fs), the transferred molecules rotated to θ=90 degrees on the B state are dominant; however, the transferred molecules rotated to θ=0 degrees on the B state should be dominant, which will probably be our next project to study.

Table 1. Parameters of the pump and probe pulses for the four cases.

Number of calculations	Intensity (W/cm^2)		Pulse duration (fs)		Energy (eV)	
	Pump	Probe	Pump	Probe	Pump	Probe
1	$1*10^{13}$	$1*10^{12}$	8	20	3.39	1.13
2	$1*10^{11}$	$1*10^{11}$	8	20	3.39	1.13
3	$1*10^{11}$	$2*10^{11}$	8	20	3.39	1.13
4	$2*10^{12}$	$1*10^{11}$	8	20	3.39	1.13

Table 2. The same Table as in Table 1, but only for pump calculations (without the probe pulse), showing how much transferred and dissociated populations are made by the only pump. The

pump parameters in the 2nd and 3rd calculations of Table 1 are the same.

Number of calculations	*Intensity (W/cm^2)*	*Pulse duration (fs)*	*Energy (eV)*	*Population of the individual states as the pump is off (at t=8 fs)*				*Dissociation on the individual electronic states*			
	Pump			P_X	P_A	P_B	P_A+P_B	V_X	V_A	V_B	Total
1	$1*10^{13}$	8	3.39	0.492	0.439	0.067	0.507013	0	9.204e-05	0.0669	0.0670276
2,3	$1*10^{11}$	8	3.39	0.985	0.011	0.003	0.014361	0	2.78e-06	0.00299	0.0030
4	$2*10^{12}$	8	3.39	0.769	0.186	0.043	0.230024	0	4.529e-05	0.0438	0.04390

IV. **Conclusions.** Photo-dissociation dynamical properties of the NaH system, including the three lowest electronic states, are studied with various intensity parameters of the pump and probe pulses. Dissociation is investigated in the 1D framework, where the second DOF (θ due to the external field), along with the angular distributions of photo-fragments of the system.

The obtained results of dissociation yields of the X and B states have oscillation behaviors due to the degeneracy points (or LICIs) owing to the energy values of the probe laser. Although the large amount of populations is transferred to the A state (from the X state), the dissociation occurs on the weak bound state B and strong bound state X due to the degeneracies created by the probe, while the values of the dissociation on the A state is almost negligible.

The fragment angular distribution of the system helped to analyze the angles at which dissociation happens. In the next project, we will focus on investigating this system for the longer delay time periods in the 1D and 2D calculations.

References

1. Max Born and W Heisenberg. Zur quantentheorie der molekeln. Original Scientific Papers Wissenschaftliche Originalarbeiten, pages 216–246, 1985. https://doi.org/10.1007/978-3-642-61659-4_16.
2. H Köuppel, Wolfgang Domcke, and Lorenz S Cederbaum. Multimode molecular dynamics beyond the born-oppenheimer approximation. Advances in chemical physics, pages 59–246 (1984). https://onlinelibrary.wiley.com/doi/book/10.1002/9780470142813.
3. Michael Baer. Beyond Born-Oppenheimer: electronic nonadiabatic coupling terms and conical intersections. John Wiley & Sons (2006).
4. Wolfgang Domcke, David R Yarkony, and Horst Köppel. Conical intersections: theory, computation and experiment, volume **17**. World Scientific (2011).
5. Fábri, Csaba and Csehi, András and Halász, Gábor and Cederbaum, Lorenz S. and Vibók, Ágnes. Classical and quantum light-induced non-adiabaticity in molecular systems. AVS QUANTUM SCIENCE, **6** (2). No. 023501 (2024). https://doi.org/10.1116/5.0191522.
6. A. Bhattacharjee and K. R. Dastidar, Phys. Rev. A, **65**, 022701 (2002). https://doi.org/10.1103/PhysRevA.65.022701.
7. M. Aymar, J. Deiglmayr and O. Dulieu, Can. J. Phys., **87**, 543 (2009). https://doi.org/10.1139/P09-005.
8. Otabek Umarov, András Csehi, Péter Badankó, Gábor J Halász, and Ágnes Vibók. Light-induced photodissociation in the lowest three electronic states of the nah molecule. Physical Chemistry Chemical Physics, **26**(8):7211–7223 (2024). https://doi.org/10.1039/D3CP05402K.
9. KR Shamasundar, Gerald Knizia, and Hans-Joachim Werner. A new internally contracted multi-reference configuration interaction method. The Journal of Chemical Physics, **135**(5) (2011). https://doi.org/10.1063/1.3609809.
10. Hans-Dieter Meyer, Fabien Gatti, and Graham A Worth. Multidimensional quantum dynamics: MCTDH theory and applications. John Wiley & Sons (2009).
11. Michael H Beck, Andreas Jäckle, Graham A Worth, and H-D Meyer. The multiconfiguration time-dependent hartree (mctdh) method: a highly efficient algorithm for propagating wavepackets. Physics reports, **324(1)**:1–105 (2000). https://doi.org/10.1016/S0370-1573(99)00047-2.